Electron grain boundary scattering and the resistivity of nanometric metallic structures

Ricardo Henriquez,[1] Simon Cancino,[2] Andres Espinosa,[1] Marcos Flores,[1] Thomas Hoffmann,[1] German Kremer,[2] Judit G. Lisoni,[1] Luis Moraga,[2] Roberto Morales,[2] Simon Oyarzun,[1] Marco Antonio Suarez,[1] Alejandro Zúñiga,[3] and Raul C. Munoz[1,*]

[1]*Departamento de Física, FCFM, Universidad de Chile, Blanco Encalada 2008, Santiago 8370449, Chile*
[2]*Centro de Física Experimental (CEFEX), Facultad de Ciencias, Universidad de Chile, Las Palmeras 3425, Santiago 7800024, Chile*
[3]*Departamento de Mecánica, FCFM, Universidad de Chile, Beauchef 850, Santiago 8370448, Chile*

(Received 20 May 2010; revised manuscript received 29 July 2010; published 23 September 2010)

The resistivity of metallic structures depends on both electron-grain boundary scattering and electron-surface scattering. By tuning the grain size, we have been able to separate the contribution to the resistivity originating in electron-grain boundary scattering, from that arising in electron-surface scattering, on gold films approximately 54 nm thick deposited onto mica substrates under high vacuum. Surprisingly, the resistivity measured between 4 and 300 K can be described by Drude's model; it can be described as well by Mayadas's theory using the grain boundary reflectivity R *as the only adjustable parameter*.

DOI: 10.1103/PhysRevB.82.113409 PACS number(s): 73.50.−h, 73.61.−r

A central issue concerning nanometric metallic structures, is how electron scattering by defects such as grain boundaries and rough surfaces gives rise to an increase in the resistivity of the structure. This century old problem[1] has sparked a debate over the last decade within the semiconductor industry,[2] and has given rise to several papers focused on this issue published over the last year alone.[3,4] Nevertheless, understanding the role that electron-surface and electron-grain boundary scattering play on the resistivity of thin metallic films today still seems fragmentary and incomplete.[5]

To elucidate the role that electron-surface and electron-grain boundary scattering play on the resistivity of metallic structures, a complete morphological and structural characterization of the samples is required. *Measurements of different charge transport coefficients through independent experiments performed on the same samples seem desirable*, to gather evidence that would permit univocal identification of the microscopic electronic scattering mechanisms giving rise to the macroscopic resistivity.

In work already published, we have measured the resistivity,[6] the Hall effect,[7] the transverse magnetoresistance,[8] and the longitudinal magnetoresistance[9] of thin gold films deposited onto mica substrates, where electron-surface scattering is the dominant electron scattering mechanism at 4 K. In the present work, by using the same sample preparation method, we have succeeded in separating electron-surface from electron-grain boundary scattering in a family of gold films evaporated onto mica substrates, simply by controlling the morphology—mainly the typical grain size—of the samples.

To achieve this goal, we started by evaporating four samples of different thickness, where the dominant electron scattering mechanism at 4 K is electron-surface scattering. The thinnest (54 nm) film became sample S4 in Table I. We then evaporated three samples of approximately the same thickness, at the same evaporation rate, *but lowering the substrate temperature* T_S. We selected three T_S such that the resistivity measured at room temperature after evaporation, differs significantly: These are samples S1, S2, and S3 in Table I. Reproducibility of resistivity versus T_S was verified preparing at least four samples of the same thickness ($\sim$50 nm) for each T_S.

Sample thickness was measured using several methods: (a) quartz crystal microbalance mounted on the high-vacuum (HV) evaporation station, (b) Rutherford backscattering, (c) profilometry, and (d) Tolansky optical interferometry, performed on glass slides placed close to the mica substrates on each run. Grain texture and orientation were determined us-

TABLE I. Morphological and electrical characterization of the samples. T_S: substrate temperature during evaporation (*: sample 4 was annealed in HV for 1 h at +270 °C after evaporation). D: average grain diameter. ΔD: standard deviation of D. t: sample thickness. d_Z: crystallite dimension along z (perpendicular to the surface of the film), determined from the width of the Au (111) diffraction peak over control samples of thickness $t^* \approx 40$ nm evaporated on the same run. h=rms. surface roughness computed on images 250 nm×250 nm, recorded with the STM. $\rho(4)$: resistivity at 4 K. $\rho(300)$: resistivity at 300 K. [In crystalline gold, the resistivity arising from electron-phonon scattering is $\rho(300)=22.5$ nΩ m]. $\Delta\rho/\rho$: transverse magnetoresistance measured at 4 K and 9 T. $\ell(4)$: distance traveled by electrons at 4 K between scattering events, according to Drude's model.

Sample	T_S (°C)	D (nm)	ΔD (nm)	t (nm)	d_Z/t^*	h (nm)	$\rho(4)$ (nΩ m)	$\rho(300)$ (nΩ m)	$\Delta\rho/\rho$ (%)	$\ell(4)$ (nm)
S1	−165	11.3	5.2	59	0.40	1.5	71.78	94.89	0.0	11.7
S2	−105	16.4	6.1	47	0.54	1.6	34.82	57.66	0.1	24.0
S3	+20	31.9	9.9	50	0.81	1.9	14.46	37.88	1.0	57.9
S4	+180*	109.7	43.9	54	0.95	3.0	7.60	32.70	3.4	110.2

 ©2010 The American Physical Society

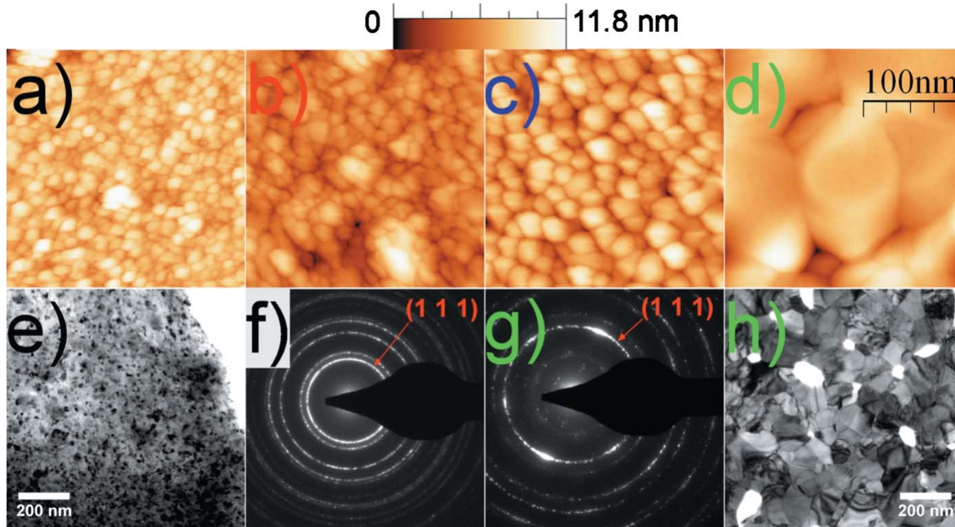

FIG. 1. (Color online) 250 nm×250 nm STM image of (a) S1; (b) S2; (c) S3; (d) S4. Vertical and horizontal scales are the same for all four images. Bright field TEM image of (e) S1 and (h) S4; Diffraction TEM pattern of (f) S1; (g) S4. In (f) and (g), (111) diffraction ring is indicated with a red (dark gray) arrow.

ing transmission electron microscopy (TEM) and x-ray diffraction. Dimensions D characterizing the diameter of the grains measured along the plane of the film were determined using scanning tunneling microscope (STM) images (over 500 grains) and compared with measurement obtained by TEM images with 5% agreement. Typical STM images are shown in Figs. 1(a)–1(d); the vertical as well as the horizontal scales are the same in all four images. TEM diffraction images and TEM bright field images are shown in Figs. 1(e)–1(h), corresponding to samples evaporated at the extreme substrate temperatures. Increasing T_S leads to increasing the grain diameter D from 11 to 110 nm, d_Z from 16 to 38 nm, and leads progressively to azimuthal grain ordering, with direction [111] of gold oriented perpendicular to the surface of the mica. On all four samples S1–S4, STM analysis at different scales (10×10 to 2000×2000 nm^2) shows a homogeneous surface (low value of rms roughness h, Table I), without voids or rugged structures. Morphological and electrical characteristics of the samples as a function of T_S are displayed in Table I.

The temperature dependence of the resistivity of S1–S4 is displayed in Fig. 3(a), transverse magnetoresistance measured at 4 K is displayed in Fig. 3(b). Following Drude's model,[10] the mean distance traveled by an electron between collisions is $\ell(T)=v_F\tau(T)$. Here $\tau(T)$ is the mean electronic collision time at temperature T, given by $\tau(T)=m^*/[nq^2\rho(T)]$, where ρ is resistivity, m^* is the electron's effective mass, q is its charge, n is the electron density, and v_F is the Fermi velocity. Cooling the sample freezes out phonons so $\ell(4)$ represents the scale of distance characterizing the structural defects that give rise to electron scattering at 4 K.

In work already published, we demonstrated that electron-surface scattering is the dominant electron scattering mechanism at 4 K, in samples evaporated at a rate of 3 nm/min, $T_S=180$ °C, annealed for 1 h at 180 or 270 °C.[7–9] In sample S4 [$\mu_H(4)$ displayed in Fig. 2, $D=110$ nm], as in samples listed in Table I of Ref. 9, we found that $\ell(4)\geq 2t$, indicating that electrons colliding with one of the surfaces limiting the film undergo a specular reflection.[9] In Fig. 2, we display the Hall mobility $\mu_H(4)$ measured at 4 K versus film thickness t, on four samples evaporated with $T_S=180$ °C and annealed for 1 h at 270 °C after evaporation. *The linear dependence of* $\mu_H(4)$ on t, allows univocal identification of electron-surface scattering as the dominant electron scattering mechanism at 4 K in S4.[7,9] Therefore, at $4<T<300$ K, the microscopic electron scattering mechanisms giving rise to the observed resistivity, are electron-surface plus electron-phonon scattering.

Regarding S1, $\ell(4)\approx D$, *suggesting that the dominant electron scattering mechanism at* 4 K *is electron-grain boundary scattering*. To verify this hypothesis, it seems appropriate to vary sample thickness while keeping D constant. Doubling the thickness for each T_S leads to a decrease in $\rho(300)$ that is 5%, 13%, 21%, and 25% for $T_S=-165$ °C, -105 °C, $+20$ °C, and $+180$ °C, respectively. For $T_S=-165$ °C, increasing thickness to $t=109$ nm, leads to a sample where $D=(13\pm 2.4)$ nm and $\rho(4)=68.7$ nΩ m, hence $\ell(4)=12.2$ nm. This confirms that *the dominant electron scattering mechanism at* 4 K *in* S1 *is, indeed, electron grain boundary scattering*. Hence, the microscopic scattering mechanisms giving rise to the resistivity of S1 at $4<T<300$ K, are electron-grain boundary plus electron-phonon scattering.

In S2 and S3, we have a crossover between the two mechanisms. The identification of $\rho_1(T)$ (resistivity of S1) as

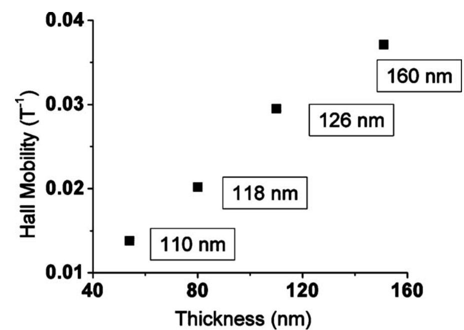

FIG. 2. Hall mobility measured at 4 K plotted versus sample thickness, for gold films evaporated at 3 nm/min onto mica substrates preheated to 180 °C, and annealed for 1 h at 270 °C after evaporation. Numbers in boxes indicate the grain diameter D.

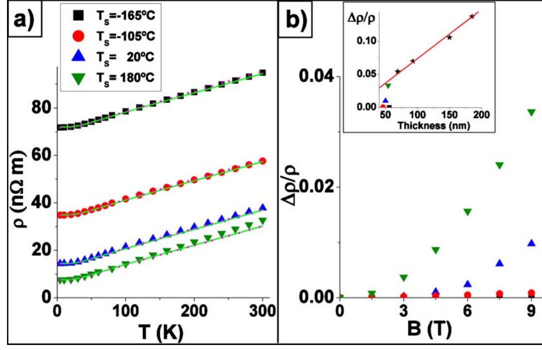

FIG. 3. (Color online) (a) Resistivity of the samples as a function of temperature. Violet (dark gray) dotted line: Drude's model. Green (light gray) solid line: Mayadas's model, with $\tau_{\rm IMP}=3.0\times10^{-12}$ s, and $P=Q=0$ for S1–S3. $R=0.37$ for S1, $R=0.28$ for S2 and $R=0.17$ for S3. For S4, $P=1$, $Q=0$, and $R=0.280$. (b) Magnetic field dependence of the transverse magnetoresistance $\Delta\rho/\rho$ observed at 4 K. Inset: thickness dependence of the transverse magnetoresistance $\Delta\rho/\rho$ observed at 4 K, 9 T, including data from Ref. 8 (black stars). In the latter as well as in S4, electron-surface scattering is the dominant electron scattering mechanism at 4 K, that leads to a linear dependence of $\Delta\rho/\rho$ (measured at 4 K, 9 T) on thickness.

arising from electron-grain boundary plus electron-phonon scattering, is coherent with the transverse magnetoresistance displayed in Fig. 3(b) (similar magnetoresistance was recently reported in porous gold films[11]). Magnetotransport provides independent experimental evidence indicating that decreasing the grain size D decreases the average electron scattering time with structural defects, thus reducing the curvature induced by the magnetic field on the electron trajectory between scattering events, thereby decreasing the magnetoresistance until—for sufficiently small D —it eventually falls below the noise level.

Increasing temperature T adds a collision time $\tau(T)_{\text{el-phon}}$ due to electron-phonon scattering. We computed $\tau(T)_{\text{el-phon}}$ using Drude's formula and the values of $\rho(T)$ for crystalline gold.[12] Adding $\tau(4)$ to $\tau(T)_{\text{el-phon}}$ yields $1/\tau(T)=1/\tau(4)+1/\tau(T)_{\text{el-phon}}$. The temperature dependent resistivity data in samples S1–S3 [where $D<\ell_0(300)$] can be accurately described by Drude's model, Fig. 3(a), using the average electron scattering time τ determined by both electron-phonon scattering plus the electron scattering time *corresponding to the scale of distance characterizing the structural defect that gives rise to electron scattering at low temperatures*, combined according to Matthiessen's rule. For S4 where $D>\ell_0(300)$, the predictions based on Drude's model underestimate the resistivity.

The first theory of resistivity including both electron-grain boundary and electron-surface scattering was published by Mayadas and Shatzkes,[13] who described electron motion using a Boltzmann transport equation. The grains were represented by a series of Dirac δ function potentials (characterized by a reflectivity coefficient R) oriented along planes perpendicular to the electric field, therefore the grains are conceived as columnar structures extending between the two surfaces limiting the metallic film. The distance separating these planes is distributed following a Gaussian, characterized by an average separation d and a standard deviation s. Current density was computed using the electron distribution functions published by Sondheimer,[14] who introduced a specularity P (representing the fraction of electrons undergoing a specular reflection upon colliding with the rough surfaces), *assuming that both surfaces limiting the film are characterized by the same specularity parameter*. The increase in resistivity induced by electron-rough surface scattering is proportional to $1-P$; electrons undergoing a specular reflection ($P=1$) *leave the resistivity unchanged*.[14]

Because our samples have different interfaces (mica and air), we modified the boundary conditions introduced by Sondheimer, to allow *two different specularity parameters P and Q* describing electron collision with the upper/lower surfaces of the film. The current density was calculated *not* employing the electron distribution functions used by Mayadas [Eq. (14) in Ref. 13 and Eq. (24) in Ref. 14] *but the distribution functions $N^{\pm}(\boldsymbol{v},z)$ used by Lucas* [Eqs. (14) and (15) in Ref. 15], replacing everywhere the bulk collision time τ (Lucas) by the "effective" collision time τ^* [Mayadas, Eq. 7(b) in Ref. 13] to account for electron-grain boundary scattering. Integration over the Fermi sphere, including the angular dependence of $N^{\pm}$ and of τ^*, yields the function $\rho/\rho_0=f\,[\ell_0(T), d, s, P, Q, R, t]$,

$$\left(\frac{\rho_0}{\rho}\right)=\frac{3}{2}\int_{-1}^{1}\frac{\tau^*(u,d,s)}{\tau}u^2du$$
$$-\frac{3\ell_0}{4t}\int_0^{2\pi}\int_0^{\pi/2}\left[\frac{\tau^*(\varsigma,d,s)}{\tau}\right]^2\frac{\cos^2(\phi)\cos(\theta)\sin^3(\theta)[1-E(\varsigma)][2-P-Q+(P+Q-2PQ)E(\varsigma)]}{1-PQE(\varsigma)^2}d\theta d\phi$$

$$\text{with}\quad u=\cos(\theta),\quad \varsigma=\sin(\theta)\cos(\phi),\quad E(\varsigma)=\exp\left(-\frac{t}{v_{\rm F}\tau^*(\varsigma,d,s)\cos(\theta)}\right),$$

$$\text{and}\quad \frac{1}{\tau^*(\varsigma,d,s)}=\frac{1}{\tau}+\frac{\ell_0}{d}\frac{R}{1-R}\frac{1}{\tau\varsigma}\frac{1-\exp[-4(\varsigma k_{\rm F})^2s^2]}{1-2\exp[-2(\varsigma k_{\rm F})^2s^2]\cos(2\varsigma k_{\rm F}d)+\exp[-4(\varsigma k_{\rm F})^2s^2]},$$

where $\rho(T)$ is the resistivity of the film, $\rho_0(T)$ is the resistivity of the bulk, $\ell_0(T)$ is the electronic mean free path in the bulk at temperature T, d and s are the average grain diameter and standard deviation characterizing the Gaussian distribution of grain sizes, respectively. R is the reflectivity characterizing grain boundaries, t is the film thickness, v_F and k_F are the Fermi velocity and wave vector. The integrals were computed by numerical integration using a 32-point Gaussian quadrature.

To analyze resistivity data, the effect of impurities in $\ell_0(T)$ was calculated using an electron-impurity scattering time $\tau_{IMP}=3.0\times10^{-12}$ s that was added—following Mattiessen´s rule—to $\tau(T)_{el\text{-}phon}$. We used the values of t listed in Table I, and of d and s obtained by fitting a Gaussian to the histogram containing D measured on each sample. For S1–S3 we set $P=Q=0$. This *maximizes the increase in resistivity attributed to electron-surface scattering in S1–S3, for a null specularity implies that electrons undergo diffuse collisions with both surfaces*. For S4 we set $P=1$ and $Q=0$, *which implies that electrons collide specularly with one of the surfaces and diffusely with the other*. Since the increase in resistivity arising from "size effects" is proportional to $1-P$, in S4 only one of the surfaces contributes to increase the resistivity.

The only fitting parameter left in the Mayadas-Lucas (ML) theory is the reflectivity parameter R; it was used to fit the 20 resistivity data points recorded for S1–S4. Notice that the resistivity of the films depends on the ratio $\ell_0(T)/t$ or $\ell_0(T)/d$. The resistivity predicted by ML is displayed in Fig. 3(a). The most interesting fit is that corresponding to S1–S3 because in these samples $D<\ell_0(300)$.

As shown in Fig. 3(a), when reducing the parameters of the theory from seven to only one— the grain boundary reflectivity R — the ML theory describes accurately the data for S1–S3. In S4—where electron-rough surface scattering plays an important role—the description provided by theory *underestimates the resistivity at higher temperatures*. Notice the progression of decreasing reflectivities required by theory to describe the resistivity data, that seem correlated with increasing azimuthal grain ordering revealed by TEM along direction [111]: $R=0.37\pm0.01$, $R=0.28\pm0.02$, and $R=0.17\pm0.02$ for S1, S2, and S3, respectively.

The resistivity predicted by Drude, seems remarkably comparable to that predicted by Mayadas. However, the results show that *the resistivity of metallic films depends not only on the distribution of grain sizes but depends as well on the probability that the wave packet representing an electron colliding with a grain boundary is either reflected backward or transmitted across the boundary*. R is proportional to this reflection probability, a property inherent to wave packets that is absent in Drude's model, and is represented in Mayadas's theory by the grain reflectivity R. *We expect that increasing crystalline misalignment between crystallites belonging to adjacent grains, as well as increasing the concentration of oxides or impurities present at grain boundaries, would increase the probability that an incoming wave packet will be reflected upon colliding with a grain boundary*. This would *increase the grain reflectivity R associated with the same distribution of grains (a Gaussian characterized by the same parameters D* and *s* in Mayadas's model), thereby increasing the resistivity of the sample.

Summarizing, in this work we have succeeded in separating and univocally identifying the role that electron-surface and electron-grain boundary scattering play on the resistivity of thin gold films. When electron-grain boundary scattering is the dominant electron scattering mechanism, the temperature dependence of the resistivity can be well described by Drude's model combined with Mathiessen's rule, or by an updated version of the theory of Mayadas and Shatzkes *involving two different specularities at the upper/lower surface of the film, where the grain boundary reflectivity R* is used as the only adjustable parameter.

Work supported by FONDECYT under Contract No. 1085026.

---

*Corresponding author; ramunoz@ing.uchile.cl

[1] I. Stone, Phys. Rev. **6**, 1 (1898); Ph. D. thesis, University of Chicago, 1898.

[2] The ITRS (International Technology Roadmap for Semiconductors) is a report published periodically by the semiconductor industry; www.itrs.net/links/.

[3] M. Wang *et al.*, J. Mater. Sci. Technol. **25**, 699 (2009); Q. Huang *et al.*, Appl. Phys. Lett. **95**, 103112 (2009); Y. Kitaoka *et al.*, *ibid.* **95**, 052110 (2009); J. S. Chawla and D. Gall, *ibid.* **94**, 252101 (2009); P. Ercius *et al.*, Microsc. Microanal. **15**, 244 (2009); A. E. Yarimbiyik *et al.*, Microelectron. Reliab. **49**, 127 (2009).

[4] T. Sun *et al.*, Phys. Rev. B **79**, 041402 (2009); **81**, 155454 (2010).

[5] This is reflected, on the one hand, on the conclusions published in 2009 regarding the resistivity data on Cu films, where it is stated that "…much of the previous work on the classical resistivity size effect, where data were interpreted as supporting a thickness-based surface scattering model, may need to be re-evaluated." (Ref. 4, p. 4). It is also reflected on the increase in resistivity arising from structural defects at 300 K [above the bulk resistivity $\rho_0(300)=17$ nΩ m of crystalline Cu], of Cu lines connecting the transistors making up an integrated circuit. For lines whose half pitch is 35 nm, in 2002 this increase was estimated to be between 30% and 55% [P. Kapur *et al.*, IEEE Trans. Electron Devices **49**, 590 (2002), Fig. 10a]. The estimation was revised *upward to approximately* 100%, 3 *years later* (Ref. 2, Fig. 68, ITRS Interconnect 2005).

[6] R. C. Munoz *et al.*, Phys. Rev. B **62**, 4686 (2000).

[7] R. C. Munoz *et al.*, Phys. Rev. Lett. **96**, 206803 (2006).

[8] R. C. Munoz *et al.*, J. Phys.: Condens. Matter **18**, 3401 (2006).

[9] R. C. Munoz *et al.*, Phys. Rev. B **81**, 165408 (2010).

[10] P. Drude, Ann. Phys. **1**, 566 (1900); N. W. Ashcroft and N. W. Mermin, *Solid State Physics* (Saunders College, New York, 1976), Chap. 1.

[11] T. Fujita *et al.*, Phys. Rev. Lett. **101**, 166601 (2008).

[12] R. A. Matula, J. Phys. Chem. Ref. Data **8**, 1147 (1979).

[13] A. F. Mayadas and M. Shatzkes, Phys. Rev. B **1**, 1382 (1970).

[14] E. H. Sondheimer, Adv. Phys. **1**, 1 (1952).

[15] M. S. P. Lucas, J. Appl. Phys. **36**, 1632 (1965).